iScience

CellPress
OPEN ACCESS

Article

Unveiling electron transfer in a supramolecular aggregate for adaptive and autonomous photochromic response

Xiaofei Kuang, Lingyi Meng, Can-Zhong Lu

czlu@fjirsm.ac.cn

Highlights

The charge transfer mechanism was unveiled between the DMA and redox-active NDI•

Supramolecular aggregation leads to stable free radical•

Significant conformational change is not necessary for reversible photochromism•

The photochromism of doped polymer film could adapt to environment autonomously

Kuang et al., iScience *24*, 102956
September 24, 2021
https://doi.org/10.1016/j.isci.2021.102956

iScience

CellPress
OPEN ACCESS

Article

Unveiling electron transfer in a supramolecular aggregate for adaptive and autonomous photochromic response

Xiaofei Kuang,[1,2,3] Lingyi Meng,[1,2,3] and Can-Zhong Lu[1,2,3,4,*]

SUMMARY

Interactive and responsive materials are dynamic molecular systems that are capable of modulating their behavior and adapting to environment autonomously. Photochromic materials are among the fascinating class of dynamic responsive systems and widely used in molecular switches and optoelectronic devices. However, the phototriggered color changing largely relies on the conformation transformation of the photochromic motif, which significantly limited their usage in organic liquid solutions. Herein, we demonstrate a photochromic organic supramolecular system by using electron-rich N,N-dimethylacetamide (DMA) and electron-deficient naphthalenediimide (NDI) as a donor and acceptor, respectively. In the binary system, the photo-induced electron transfer through lone pair$\cdots\pi$ interactions pathway leads to dynamic photochromic response not only in the solution but also in the crystalline aggregated state. Furthermore, by incorporating the supramolecules in the polymer matrix, the transparent polymeric film also exhibits rapid photochromic response, which makes it a promisingly interactive and adaptive photochromic material.

INTRODUCTION

During the past decades, there has been tremendous interest in dynamic molecular systems such as molecular machine, motor, rotor, and switch, which could sense and respond to external stimulus such as light, heat, pH, and mechanical force, as well as perform smart functions (Štacko et al., 2017; Chen et al., 2018; Li et al., 2020; Moulin et al., 2020; Corra et al., 2020; White and Broer, 2015; Karothu et al., 2020; McCracken et al., 2020; Goulet-Hanssens et al., 2020). Although the classic stimuli-responsive materials are generally considered as smart materials, they lack the ability to sense and adapt to the surrounding environment and act autonomously for advanced function because the outside triggers or energy inputs are required to drive the dynamic responsive performance (Zhang et al., 2019; Merindol and Walther, 2017; McCune et al., 2020). In fact, some natural species are prototypical, sophisticated, and intelligent systems with self-regulated, autonomous, and adaptive actions. For example, the organisms could sense the environment temperature and sustain their life by thermoregulation. The elastic lens of human eye could change their curvatures by the relaxation or contraction of the ciliary muscle for optical imaging of the objects on the retina varying from distant to nearby. It is thus a contemporary challenge and forefront to mimic the nature to construct artificially interactive and adaptive materials with an advanced intelligent system, which enables the capabilities of emergent life-like behaviors (Priimagi and Hecht, 2020; Walther, 2020; Feringa, 2020; Lancia et al., 2019).

Among the fruitful dynamic behaviors in nature, color change capabilities play a crucial role in the survival of certain animals. Pertinent examples are chameleons and the cephalopods animals such as squid and cuttlefish, and they possess the extraordinary ability to change the skin color in an instant to camouflage and adapt to the surrounding (Teyssier et al., 2015; Morin et al., 2012; Xu et al., 2018; Isapour and Lattuada, 2018). Inspired by the remarkably dynamic and adaptive capabilities, various photochromic artificial molecular devices have been exploited owing to their intriguing structural features and fascinating applications in the fields of molecular switches, data recording, ophthalmic lenses, and biological probes (Orgiu and Samorì, 2014; Hou et al., 2019; Evans et al., 2005; Wang and Li, 2018; Li et al., 2014; Ma et al., 2020a; 2020b; Zhang et al., 2017; Ma et al., 2020a, 2020b; Jiang et al., 2021). Typical photochromic molecular species, including dithienylethenes, azobenzenes, spiropyrans, and stilbenes, have been intensively investigated

[1]Xiamen Key Laboratory of Rare Earth Photoelectric Functional Materials, Xiamen Institute of Rare Earth Materials, Haixi Institutes, Chinese Academy of Sciences, Xiamen 361021, P. R. China

[2]CAS Key Laboratory of Design and Assembly of Functional Nanostructures, and Fujian Key Laboratory of Nanomaterials, Fujian Institute of Research on the Structure of Matter, Chinese Academy of Sciences, Fuzhou, Fujian 350002, P. R. China

[3]University of Chinese Academy of Sciences, Beijing 100049, P. R. China

[4]Lead contact

*Correspondence: czlu@fjirsm.ac.cn

https://doi.org/10.1016/j.isci.2021.102956

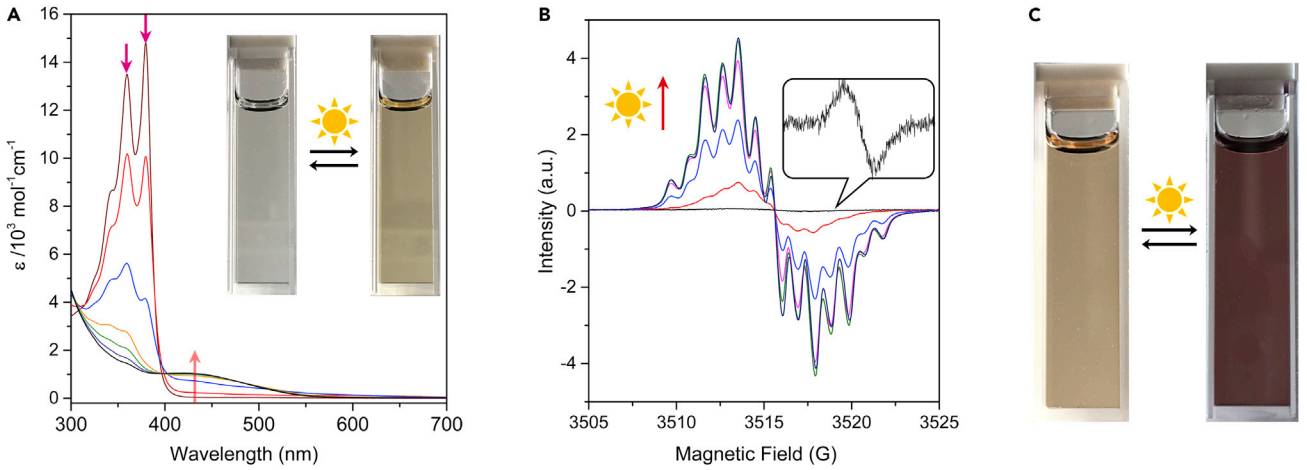

Figure 1. Dynamic spectroscopic analysis and photochromic behavior of NDI in DMA solution

(A) Dynamic UV/visible absorption spectra of NDI in DMA dilute solution (2×10^{-4} M) upon irradiation using a 300 W xenon lamp for 3 min at 30-s intervals. Inset: the reversible photochromic behavior of color changes for the dilute solution.

(B) Dynamic ESR spectra of NDI in DMA saturated solution (5.5×10^{-3}M) upon irradiation using a 300-W xenon lamp for 50 s at 10-s intervals. Inset: ESR spectrum of the sample without light irradiation.

(C)The photochromic behavior of NDI in DMA saturated solution (5.5×10^{-3}M) upon light irradiation using a 300-W xenon lamp for 1 min.

so far (Zhang et al., 2013; Irie et al., 2014; Kortekaas and Browne, 2019). Nevertheless, it is inevitable that significantly geometrical configuration change during the photo-induced color change process in these systems, which largely confine the dynamic photochromic behavior in solution or in the matrix, because the tight molecular packing in the crystalline or aggregated state restrains the isomerization of the active motifs (Kuroiwa et al., 2019; Ma et al., 2019; Chen et al., 2020). Although many strategies have been developed to overcome this issue (Torres-Pierna et al., 2020; Vázquez-Mera, et al., 2013; Long et al., 2014), for example, Abe et al. designed the imidazole-based molecular species with minimal conformation change (Kometani et al., 2020; Usui et al., 2020), while others provide flexible and soft host matrix to facilitate isomerization of the active motif in the confined space (Samanta et al., 2018; Williams et al., 2018), it is highly desirable to exploit a novel photochromic system that could fast respond to the light without altering the molecular framework and could be easily fabricated from readily available precursors, such as the extensively investigated redox-active viologen complexes (Liu et al., 2021; Chen et al., 2017; Li et al., 2019) and, more importantly, have the capability to sense and adapt to the external environment for autonomous function. Herein, we report a dynamically responsive and environment compatible photochromic system by taking advantage of the planar, aromatic π-conjugated structural feature of naphthalenediimide (NDI) and its inherent redox activity.

RESULTS AND DISCUSSION

Spectroscopic properties of N,N-dimethylacetamide-NDI in the solution state

In our previous work for the preparation of **Cu-NDI** supramolecular network, by exposing the NDI in N,N-dimethylacetamide (DMA) solution in the sunlight, the brown solution became dark red and it could last for a long time (Kuang et al., 2019). This serendipitous phenomenon motivated us to illuminate the electronic communications in the binary solution system by spectroscopic evidence (Scheme S1). UV/visible absorption spectrum in DMA displays π-π* transition absorption peaks at 360 nm and 379 nm (Figure 1A), which is characteristic NDI absorption in the ground state. Dynamic excited-state electron transfer was monitored by means of UV/visible spectroscopy; upon continuous irradiation using a 300-W xenon lamp for 3 min with 30-s interval, the absorption spectra underwent drastic changes with the main peaks at 360 nm and 379 nm progressively disappearing and a broad charge transfer absorption band concomitantly emerging at long wavelengths, which are characteristic of the charge transfer $NDI^{\bullet -}$ species (Song et al., 2015). In the light irradiation process, the absorption spectra established a clear isosbestic point at 395 nm along with the colorless solution converted into light yellow. The photochromic color change and broad charge transfer absorption in the visible region confirmed the photo-induced partial electron transfer in the dilute solution system.

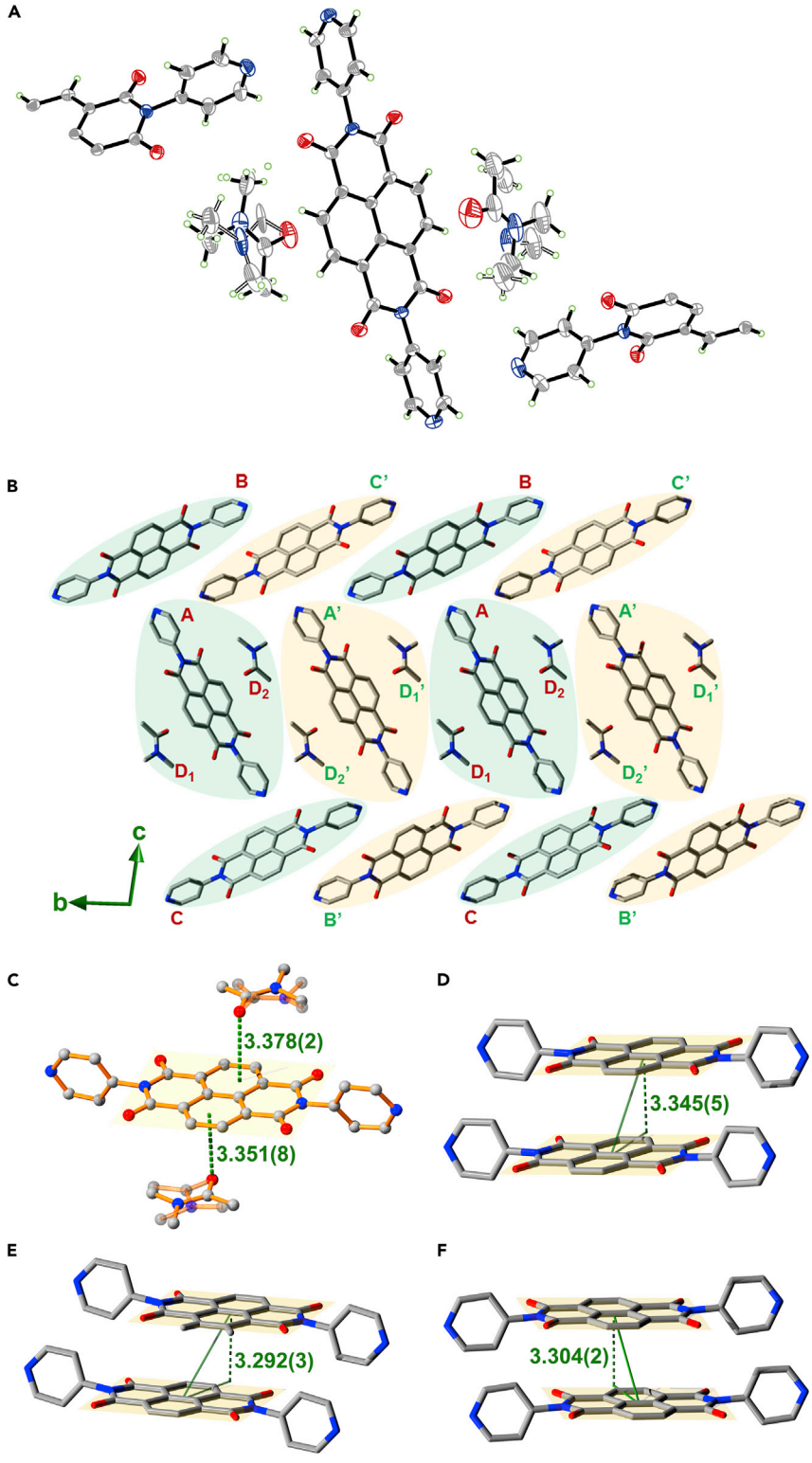

Figure 2. Single-crystal structure analysis of organic cocrystal DMA-NDI

(A) The asymmetric unit of DMA-NDI with thermal ellipsoid (with 50% probability), where nitrogen and oxygen are highlighted in blue and red, respectively.

Figure 2. *Continued*
(B) View shown the supramolecular arrangement of the cocrystal **DMA-NDI** from *a*-axis. The five-component structural units are represented by green or yellow ellipses, and their corresponding units are centrosymmetric.
(C) The two DMA moieties locate on each side of π-plane of **A** motif through O lone pair···π interactions.
(D) Supramolecular π···π stacking of **A** motifs.
(E) Supramolecular π···π stacking of **B** motifs.
(F) Supramolecular π···π stacking of **C** motifs.

To further vindicate the dynamic photo-induced electron transfer and visualize the photochromic behavior, a concentrated saturated solution (5.5×10^{-3}M) was prepared; it is noteworthy that the occurrence of a week radical signal with g factor of 2.0043 was detected by electron spin resonance (ESR) in the ground state as shown in Figure 1B. Upon light irradiation for 1 min, the intensity of the ESR signal increased simultaneously and the brown solution immediately turned into dark red (Figure 1C). This means that spontaneous ground-state partial charge transfer existed in the concentrated solution and photo-triggered excited-state electron transfer both in dilute and concentrated solutions.

X-ray crystallography analysis of cocrystal DMA-NDI

Based on the photo-induced electron transfer and photochromic behavior in the solution, it is intriguing to investigate their electronic interactions in the solid state from crystal engineering point of view because charge transfer cocrystals usually assembled from electron-donating and electron-accepting individuals through a specific supramolecular arrangement (Sun et al., 2019). Fortunately, suitable crystals were prepared by recrystallizing the saturated solution of NDI in DMA in a sealed beaker in dark for two weeks. Single-crystal X-ray diffraction analysis indicates that the prepared organic solid is binary solvated cocrystal (**DMA-NDI**) which crystalizes in the P-1 space group. The asymmetric unit contains one crystallographically independent (**A**) and two halves of NDI species (**B** and **C**) as well as two discrete DMA units ($\mathbf{D_1}$ and $\mathbf{D_2}$) (Figure 2A). In the supramolecular assemblies, the **A** motif stacks with **B** and **C** species in a herringbone packing mode with each of pyridine ring direction and is further sandwiched with two DMA species in each side of its π-plane forming a five-component supramolecular adduct ($\mathbf{BD_1AD_2C}$) (Figure 2B). The supramolecular adduct ($\mathbf{BD_1AD_2C}$) further stacks with the identical but crystallographically centrosymmetric supramolecular adduct ($\mathbf{B'D_1'A'D_2'C'}$) alternatively, generating a one-dimensional (1D) supramolecular column.

It is noteworthy that close contact was observed between the O atoms of the DMA and NDI plane in **A** motif (d_1 = 3.378(2)Å, d_2 = 3.351(8)Å), which means obvious lone pairs···π interactions in the supramolecular adduct (Figure 2C). The propagation of the assembly is extended by alternating stacking of the supramolecular column in a herringbone mode forming a 2D layer in the *bc* plane through C-H···π interactions and further stacking into an ordered J-aggregated 3D supramolecular architecture through close π···π packing of each **A**, **B,** and **C** of NDIs motifs in a slipped-stacking arrangement along the *a*-axis direction. The π···π distances of each individual **A**, **B,** and **C** motif are 3.345(5)Å, 3.292(3)Å, and 3.304(2)Å, respectively (Figures 2D–2F). The completed 3D organic cocrystal is stabilized by π···π, C-H···π interactions and C-H···O hydrogen bonds (Figure S1 supplementary information).

ESR spectra characterization of the $NDI^{\bullet-}$ radical anions in the solid state

In the context of photo-induced electron transfer in solution state and further structural insights into the binary solvated cocrystal, it arouses our great attention to shed light on the donor and acceptor electronic structural feature in the solid state. To unveil the electron transfer mechanism and photochromic behavior of the supramolecular system, ESR spectra were recorded to provide direct evidence of unpaired electrons in solid-state cocrystal of **DMA-NDI**. Remarkably, an obvious and sharp resonance signal centered at g = 2.0043 was observed under ambient condition (Figure 3A). It distinctly indicates that the existence of stable and active $NDI^{\bullet-}$ radical anions in the **DMA-NDI** originated from ground-state partial charge transfer. In order to elucidate the excited-state photo-induced electron transfer process, *in situ* ESR measurements were performed by continuous light irradiation simultaneously on this solid-state sample. After the light irradiation for 2 min, the radical signal intensity drastically increased, and in the subsequent 2-14 min, the intensity slightly increases until saturation. This dynamic behavior of ESR spectra upon continuous light irradiation unambiguously indicates the photo-induced electron transfer in the cocrystal.

Temperature-dependent ESR spectra were also performed to further check the thermal susceptibility of the intrinsic radical ions. At low temperature of 100 K, there are still stable and persistent free radical

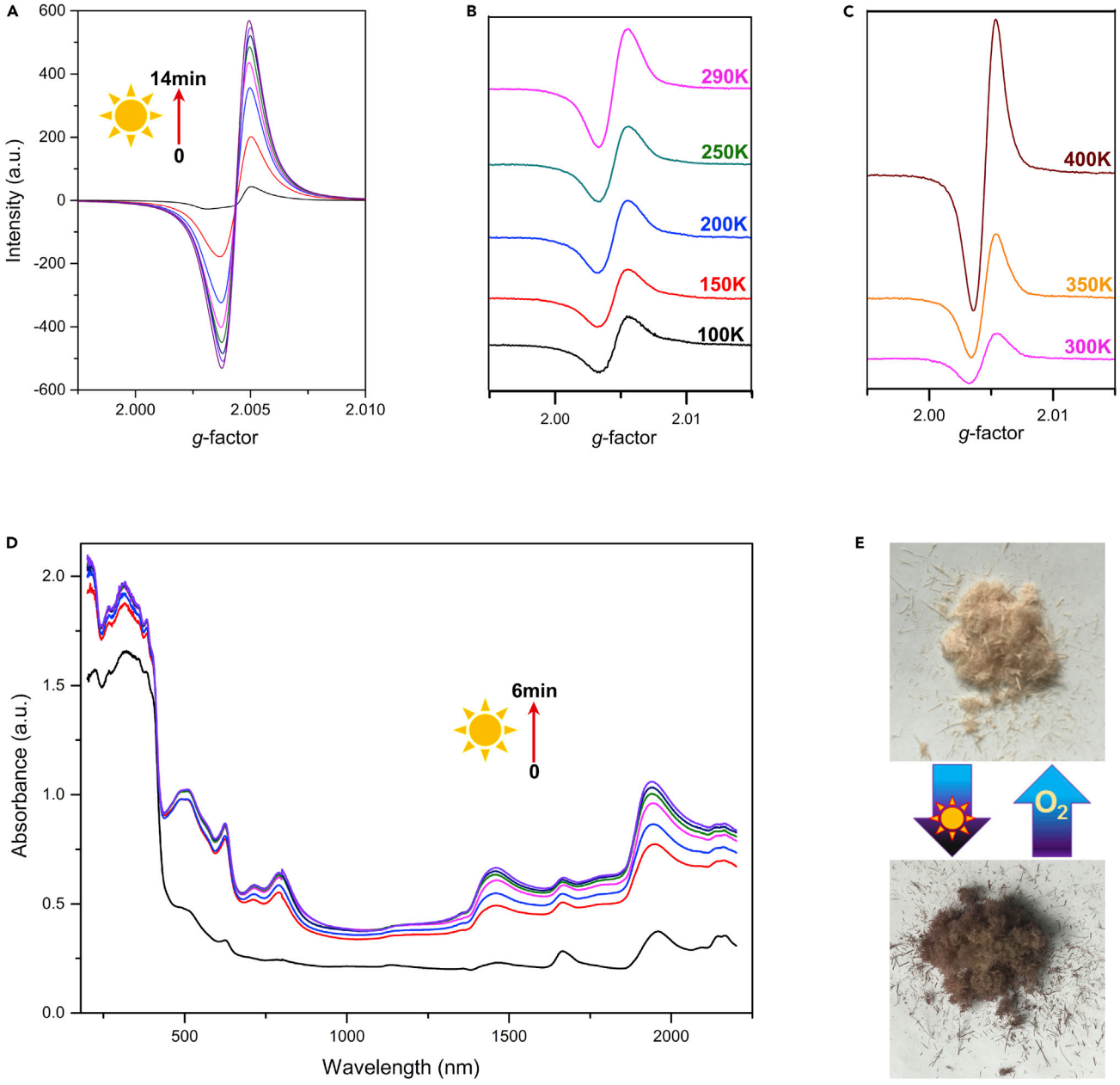

Figure 3. Dynamic spectroscopic and ESR properties and photochromic behavior of DMA-NDI cocrystal

(A) The *in situ* dynamic ESR spectra of **DMA-NDI** upon irradiation using a 300-W xenon lamp for 14 min at 2-min intervals. The black curve represents the intrinsic ground-state ESR signal, and the colored curves are excited-state ESR signals.

(B)The variable temperature ESR from 100 K to 290 K.

(C)The variable temperature ESR from 300 K to 400 K.

(D)The *in situ* dynamic solid-state diffuse reflectance spectra of **DMA-NDI** upon irradiation using a 300-W xenon lamp for 6 min at 1-min intervals. The black curve represents the ground-state absorption spectrum, and the colored curves are excited-state absorption spectra.

(E)The reversible photochromic behavior of **DMA-NDI**.

ions, and while elevating of the temperature to 290 K, the intensity of the signal becomes stronger (Figure 3B). Moreover, the same batch of sample was also investigated above the room temperature; the intensity of the radical signal greatly enhanced when increasing the temperature to 400 K (Figure 3C). The behavior reveals that the intrinsic radical is also stable at low temperature and thermally promoted dynamic electron transfer between the donor and acceptor cocrystal of **DMA-NDI**.

Solid-state diffuse reflectance spectra characterization of the electron transfer

To address the correlation between the solid-state crystal structure and dynamic electron transfer mechanism, solid-state spectroscopic measurements were also carried out by *in situ* diffuse reflectance spectrum. Compared with the absorption spectra in the dilute solution, solid-state absorption spectrum of the cocrystal **DMA-NDI** displayed new absorption bands which centered at 500 nm, 622 nm, 710 nm, and 790 nm in the visible region and at 1455 nm, 1666 nm, 1945 nm, and 2152 nm in the near-infrared (IR) region under ambient condition (Figure 3D). The emergence of new absorption bands may be attributed to some degree of charge transfer interactions and π-stacking excitonic coupling between the electron-donating DMA and electron-accepting NDI in the crystalline state. The new emergence of absorption bands in visible and near-IR regions further confirmed that the molecular interactions is quite different from in the solution state and the charge transfer interactions seems to be enhanced after cocrystallization of the DMA and NDI.

Upon light irradiation using a 300-W xenon lamp for 1 min, the intensity of the absorption band increased dramatically from UV to near-IR range, especially the well-defined absorption band centered at 1455 nm, 1666 nm, and 1945 nm in the near-IR region. This implies that the cocrystal is highly sensitive and fast responsive to light and rapid photo-driven excited-state electron transfer. Moreover, upon continuous irradiation with the prolongation of the time till 6 min, the intensity of the absorption band increases gradually with duration of irradiation and finally tends to saturation with strong near-IR absorption at 1945 nm (Figure 3D). The electron transfer phenomenon is also visualized by color change from light gray to dark gray, which means that the cocrystal also exhibits the photochromic behavior (Figure 3E). The reversible photochromism can be recovered by storing the sample in air for 10 hr at ambient condition (Han et al., 2013; Liu et al., 2015). Furthermore, the organic cocrystal could be stable in 100°C under ambient conditions (Figure S2) and there are no clear structural changes during the reversible photochromic cycles, which was confirmed by the IR spectra and powder X-ray diffraction (PXRD) before and after light irradiation (Figures S3 and S4).

Density functional theory calculation of the electron interactions and energy diagrams

In order to gain a further understanding of the electronic structure properties of the donor and acceptor system, density functional theory (DFT) is used to calculate the single-point energy and analyze the electronic structure with the functional B3LYP combining with the basis set 6-311+G(d,p) for C, H, N, and O atoms. The calculations demonstrate that the highest occupied molecular orbital (HOMO) is localized on the electron-donating DMA moiety, while the lowest unoccupied molecular orbital (LUMO) is localized on the electron-accepting NDI unit (Figure 4A). DFT calculations of the energy diagrams reveal that the HOMO of cocrystal is −6.87 eV, which is similar to the DMA HOMO (−6.85 eV) and that the cocrystal LUMO (−3.74 eV) is closer to the NDI LUMO (−3.78 eV) (Figure 4B). In this scenario, for the discrete solution system, the HOMO of electron donor DMA falls below the LUMO of the NDI but still lies above its HOMO; light could activate the NDI moieties to form the photogenerated NDI* excited state. By this way, electron transfer turns on from DMA HOMO to NDI singly occupied molecular orbital (SOMO) through the photo-induced electron transfer pathway, generating radical anions $NDI^{\bullet-}$ as confirmed by the UV/visible spectroscopy.

The ground-state charge transfer and excited-state electron transfer mechanism

By comprehensive analysis of the dynamic UV/visible spectroscopy and ESR spectra in solution and solid state as well as theoretical insights into the cocrystal, it unequivocally demonstrates that the solvent molecule DMA behaves as a latent electron-donating reducing regent in the supramolecular system. In the ground state for the dilute solution, there are no obvious charge transfer interactions because the HOMO energy level of the electron-donating DMA is located between the HOMO and LUMO energy level of electron-accepting NDI; however, with the assistance of the light driving, electron transfer turns on, which is accompanied with obvious color change. Nevertheless, in highly concentrated saturated solution, spontaneous charge transfer occurs so that ambient stable radical anions exist in the supramolecular system. The phenomena could be interpreted by the matched HOMO energy levels of DMA and NDI and aggregation-induced effect. In the dilute solution state, the NDI molecules are highly disordered dispersed in the solution with random motion, the week electron donating ability of DMA need the external stimuli such as light to activate the NDI acceptor for effective charge transfer. However, in the concentrated solution or crystalline state, the NDI motifs are highly ordered stacked through π···π interactions and Coulombic attraction, so close molecular contacts between the donor and acceptor with specific charge transfer

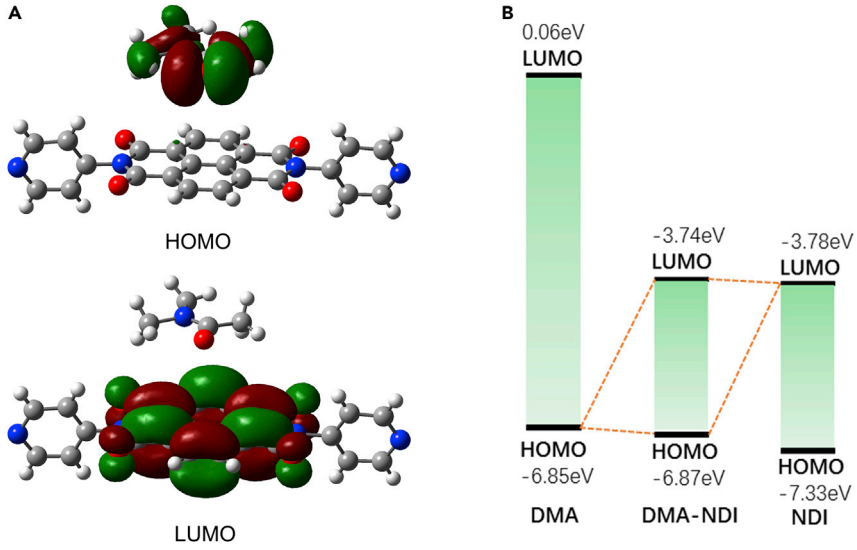

Figure 4. DFT calculations of the electronic structural properties of DMA-NDI

(A) The electron density of HOMO and LUMO in **DMA-NDI**.

(B) The energy level diagram of **DMA**, cocrystal **DMA-NDI**, and **NDI**.

pathway render spontaneous charge transfer in the supramolecular aggregate. The inference was confirmed by the straightforward single-crystal structural analysis in which two electron-donating DMA moieties were located on each side of the NDI π-plane through lone pairs···π interactions. The electron-rich O lone pairs in DMA to electron-deficient NDI π-plane provides direct charge transfer pathway and leads to generating stable free radicals both in the concentrated solution and solid state even at a low temperature. The synergistic effect of week electron-donating DMA and specific lone pairs···π charge transfer pathway as well as ordered supramolecular aggregation endow the organic cocrystal with stable free radicals both in the ground state and excited state, which enables it fast light or thermal response and reversible photochromic behavior.

Autonomous and dynamic photochromic response of NDI-doped polymer matrix

The aforementioned results of the supramolecular electron transfer and unique reversible redox activity driven by the light and recovered by O_2 in the air impart it a promising dynamic responsive photochromic materials which could sense external environment because the light and air are ubiquitous in nature. Systems chemistry enables the integrating the individual molecular components into a hierarchical and sophisticated system with higher levels of complexity, and ultimately, the cooperative effects impart the materials with advanced functionalities (Azevedo et al., 2020). Benefit of the photochromic behavior both in the solution and in the solid state and inspired by the crystallization in confinement strategy (Yoreo et al., 2015; Meldrum and O'Shaughnessy, 2020), we try to embed the active NDI motif in polymer matrix by using DMA as solvent. Owing to the high solubility of both NDI and polymer matrix in DMA, the colorless and transparent film was fabricated by dispersing NDI in poly(methyl methacrylate) (PMMA) matrix. Upon light irradiation for 1 min, the transparent doped polymeric film immediately changes its color from colorless to dark brown (Figures 5A and S6). To further investigate the light-responsive dynamics of the polymeric film, we also perform the UV-visible spectroscopy to monitor the photochromic performance. In the ground state, intense absorption bands appear in the UV region, as similar to the solution and solid state of the supramolecules; furthermore, there are weak absorption bands in the near-IR region at 1680 nm, 1908 nm, and 2140 nm, which are characteristic bands analogous to the solid-state cocrystal. In addition, there are new and intense absorption peaks emerged at a long wavelength region centered at 2250 nm, 2770 nm, and 2905 nm (Figure 5B). Upon light irradiation for 30 s, the color of the polymeric film immediately changed from colorless to dark brown and further irradiation till 4 min led to coloration saturation. In this process, new charge-transfer absorption bands emerged at 472 nm, 606 nm, 780 nm, and 1170 nm, and the absorption intensity at 1680 nm, 1908 nm, 2140 nm, 2250 nm, and 2370 nm increases, accompanied by extending the irradiation time,

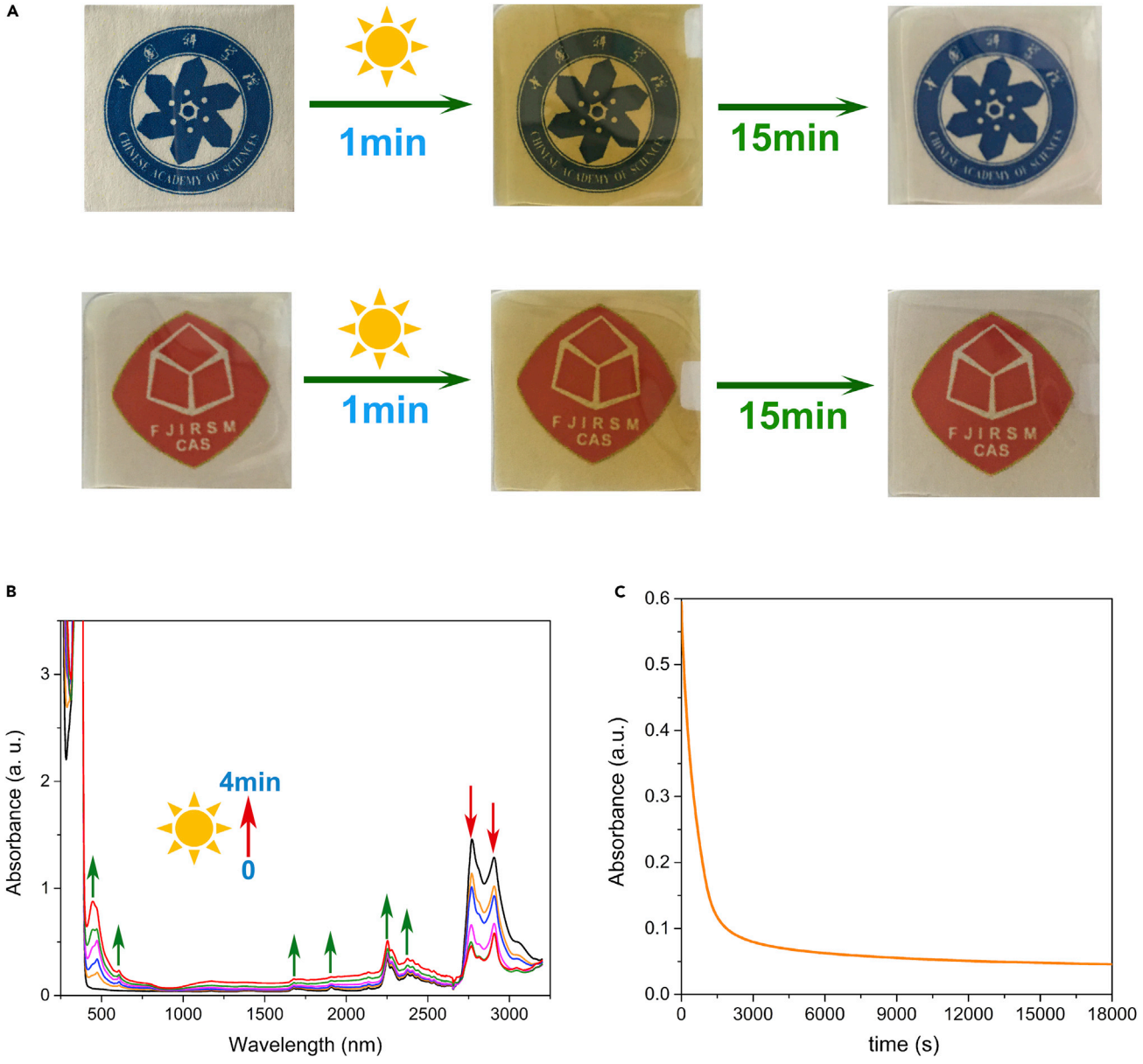

Figure 5. The photochromic behavior of NDI-doped polymer matrix

(A) The initial and second coloration and discoloration cycle of the same transparent polymeric film on the different pattern.

(B) The *in situ* dynamic absorption spectra of NDI-doped polymer matrix upon irradiation using a 300-W xenon lamp for 4 min. The black curve represents the ground-state absorption spectrum, and the colored curves are excited-state absorption spectra with irradiation for 30 s, 1 min, 2 min, 3 min, and 4 min.

(C) The fading kinetics curve of the NDI-doped polymer matrix after removing the light source. The absorbance was monitored at 472 nm.

while at 2770 nm and 2905 nm, the absorption intensity decreases concurrently, indicating the formation of colored anion radical state. Figure 5C shows the fading kinetics of the doped polymeric films at λ = 472 nm after the removal of the light source. The fading curve for the transient absorbance was fitted by standard biexponential model which fulfills the function: $A(t) = A_1e^{-k_1t} + A_2e^{-k_2t} + A_{th}$. The fitted decay curve demonstrates that the rate constants are $k_1 = 1.68 \times 10^{-3}s^{-1}$ and $k_2 = 1.51 \times 10^{-4}s^{-1}$ (Figure S5), and the half-lives ($\tau_{1/2}$) of the doped polymer film is 528 s under ambient condition (Evans et al., 2005; Kuroiwa et al., 2019).The fast-decay component attributes to the primary reduced $NDI^{\bullet-}$ radical species, while the slow-decay component arises from the further reduced NDI^{2-} species during the continuous photo-induced electron transfer process.

Generally, the integration of the active photochromic motifs in polymer matrices is far more for practical applications. However, this would significantly obtund the light response, which arises from the inhibition of the conformational changes for the active motifs by steric hindrance of the polymer matrices. Nonetheless, in the polymer confined crystalline system, embedding of the **DMA-NDI** in polymer matrix dramatically improves the photochromic response compared with that in its corresponding solution and solid state, especially for the fading performance. The enhanced light response attributes to the inherent molecular structure and intrinsic electron transfer mechanism during the redox process and the homogeneous dispersion of the microcrystals and nanocrystals in the polymer matrix, which substantially increases the exposure for coloration and the oxygen permeability for the discoloration in the dark. Moreover, to evaluate the durability and robustness of the transparent photochromic polymeric film, the light irradiation coloration and the spontaneous fading cycle were repeated multiple times (Figure S7), which manifest the high fatigue resistance of the materials without degradation of the active species. Additionally, by exposing the transparent polymeric film to natural sunlight for 1 min, the color changes to dark brown and fades in 30 min in the indoors (Figure S8). This further demonstrates that the doped polymeric film is a smart and interactive functional material which could autonomously respond to natural light and adapt its photochromic behavior in accordance with the surrounding environment.

CONCLUSION

In summary, we have demonstrated an interactive and autonomously responsive photochromic supramolecular system and deciphered a solvent-mediated electron transfer mechanism through lone pair$\cdots\pi$ interactions. The DMA behaved as a latent electron donor for the supramolecular pair in the dilute solution, and electron transfer could be triggered by photo driving. In the concentrated solution or solid state, spontaneous charge transfer induces the formation of ambient stable radicals, which originated from close molecular contacts and matched pairs of frontier orbitals as well as ordered molecular aggregation. We envision that our finding provides deep mechanistic insights into photo-induced lone pair$\cdots\pi$ electron transfer and inspires the development of organic optoelectronic devices. Furthermore, conventional organic materials suffered from tedious synthetic procedures and significant conformational change as well as photobleaching during the photochromic process. The low-cost, green synthesis, metal-free, and solution-processed supramolecular assemblies and remarkably dynamical response enable the straightforward and scalable fabrication of highly transparent photochromic films for advanced adaptive, interactive and compatible materials in military service, anticounterfeiting, smart windows, and so on.

Limitations of the study

The current research unveiled the charge transfer mechanism between the donor and acceptor supramolecular pair of DMA and NDI. However, the solid-state UV-vis spectra of cocrystal were not available beyond 2200 nm in the near-IR region, which is essential to make a comparison and understand the supramolecular interactions between the supramolecular pair and the polymer matrix.

STAR★METHODS

Detailed methods are provided in the online version of this paper and include the following:

- KEY RESOURCES TABLE
- RESOURCE AVAILABILITY
  - Lead contact
  - Materials availability
  - Data and code availability
- METHOD DETAILS
  - Synthesis and preparation
  - Characterizations
  - X-ray crystallography
  - UV/visible and NIR spectroscopy
  - Electron spin resonance spectroscopy
  - Dynamic fading curves of the NDI-doped polymeric film
  - Computational details

SUPPLEMENTAL INFORMATION

Supplemental information can be found online at https://doi.org/10.1016/j.isci.2021.102956.

ACKNOWLEDGMENTS

This work was supported by the Strategic Priority Research Program of the Chinese Academy of Sciences (XDB20000000), the Key Program of Frontier Science, Chinese Academy of Sciences (QYZDJ-SSW-SLH033), the National Natural Science Foundation of China (21701177, 21521061, 52073286, 51672271, and 21773246), and the Natural Science Foundation of Fujian Province (2006L2005 and 2019J01123).

AUTHOR CONTRIBUTIONS

X. K. and C-.Z.L. conceived the idea and designed the research. X.K. performed the experiment and analyzed the data. L.M. conducted the theoretical calculation. X.K. drafted the manuscript, and C-.Z.L. supervised the project.

DECLARATION OF INTERESTS

The authors declare no competing interests.

Received: January 26, 2021
Revised: July 9, 2021
Accepted: August 2, 2021
Published: September 24, 2021

REFERENCES

Azevedo, H.S., Perry, S.L., Korevaar, P.A., and Das, D. (2020). Complexity emerges from chemistry. Nat. Chem. *12*, 793–794.

Chen, C., Sun, J.-K., Zhang, Y.-J., Yang, X.-D., and Zhang, J. (2017). Flexible viologen-based porous framework showing X-ray induced photochromism with single-crystal-to-single-crystal transformation. Angew. Chem. Int. Ed. *56*, 14458–14462.

Chen, J., Leung, F.K.-C., Stuart, M.C.A., Kajitani, T., Fukushima, T., Giessen, E., and Feringa, B.L. (2018). Artificial muscle-like function from hierarchical supramolecular assembly of photoresponsive molecular motors. Nat. Chem. *10*, 132–138.

Chen, X., Zhao, W., Baryshnikov, G., Steigerwald, M.L., Gu, J., Zhou, Y., Ågren, H., Zou, Q., Chen, W., and Zhu, L. (2020). Engineering stable radicals using photochromic triggers. Nat. Commun. *11*, 945.

Corra, S., Curcio, M., Baroncini, M., Silvi, S., and Credi, A. (2020). Photoactivated artificial molecular machines that can perform tasks. Adv. Mater. *32*, 1906064.

Dinolfo, P.H., Williams, M.E., Stern, C.L., and Hupp, J.T. (2004). Rhenium-based molecular rectangles as frameworks for ligand-centered mixed valency and optical electron transfer. J. Am. Chem. Soc. *126*, 12989–13001.

Evans, R.A., Hanley, T.L., Skidmore, M.A., Davis, T.P., Such, G.K., Yee, L.H., Ball, G., and Lewis, D.A. (2005). The generic enhancement of photochromic dye switching speeds in a rigid polymer matrix. Nat. Mater. *4*, 249–253.

Feringa, B.L. (2020). Vision statement: materials in motion. Adv. Mater. *32*, 1906416.

Frisch, M.J., Trucks, G.W., Schlegel, H.B., Scuseria, G.E., Robb, M.A., Cheeseman, J.R., Scalmani, G., Barone, V., Mennucci, B., Petersson, G.A., et al. (2009). Gaussian 09 (Gaussian Inc.).

Goulet-Hanssens, A., Eisenreich, F., and Hecht, S. (2020). Enlightening materials with photoswitches. Adv. Mater. *32*, 1905966.

Han, L., Qin, L., Xu, L., Zhou, Y., Sun, J., and Zou, X. (2013). A novel photochromic calcium-based metal–organic framework derived from a naphthalene diimide chromophore. Chem. Commun. *49*, 406–408.

Hou, L., Zhang, X., Cotella, G.F., Carnicella, G., Herder, M., Schmidt, B.M., Patzel, M., Hecht, S., Cacialli, F., and Samorì, P. (2019). Optically switchable organic light-emitting transistors. Nat. Nanotechnol. *14*, 347–353.

Irie, M., Fukaminato, T., Matsuda, K., and Kobatake, S. (2014). Photochromism of diarylethene molecules and crystals: memories, switches, and actuators. Chem. Rev. *114*, 12174–12277.

Isapour, G., and Lattuada, M. (2018). Bioinspired stimuli-responsive color-changing systems. Adv. Mater. *30*, 1707069.

Jiang, X.-F., Han, S.-D., Wang, A.-N., Pan, J., and Wang, G.-M. (2021). The tri(imidazole)-derivative moiety: a new category of electron acceptors for the design of crystalline hybrid photochromic materials. Chem. Eur. J. *27*, 1410–1415.

Karothu, D.P., Halabi, J.M., Li, L., Colin-Molina, A., Rodríguez-Molina, B., and Naumov, P. (2020). Global performance indices for dynamic crystals as organic thermal actuators. Adv. Mater. *32*, 1906216.

Kometani, A., Inagaki, Y., Mutoh, K., and Abe, J. (2020). Red or near-infrared light operating negative photochromism of a binaphthyl-bridged imidazole dimer. J. Am. Chem. Soc. *142*, 7995–8005.

Kortekaas, L., and Browne, W.R. (2019). The evolution of spiropyran: fundamentals and progress of an extraordinarily versatile photochrome. Chem. Soc. Rev. *48*, 3406–3424.

Kuang, X., Chen, S., Meng, L., Chen, J., Wu, X., Zhang, G., Zhong, G., Hu, T., Li, Y., and Lu, C.-Z. (2019). Supramolecular aggregation of a redox-active copper-naphthalenediimide network with intrinsic electron conduction. Chem. Commun. *55*, 1643–1646.

Kuroiwa, H., Inagaki, Y., Mutoh, K., and Abe, J. (2019). On-demand control of the photochromic properties of naphthopyrans. Adv. Mater. *31*, 1805661.

Lancia, F., Ryabchun, A., and Katsonis, N. (2019). Life-like motion driven by artificial molecular machines. Nat. Rev. Chem. *3*, 536–551.

Li, K., Xiang, Y., Wang, X., Li, J., Hu, R., Tong, A., and Tang, B.Z. (2014). Reversible photochromic system based on rhodamine B salicylaldehyde hydrazone metal complex. J. Am. Chem. Soc. *136*, 1643–1649.

Li, S.-L., Han, M., Zhang, Y., Li, G.-P., Li, M., He, G., and Zhang, X.-M. (2019). X-ray and UV dual photochromism, thermochromism, electrochromism, and amine-selective chemochromism in an anderson-like Zn_7 cluster-based 7-fold interpenetrated framework. J. Am. Chem. Soc. *141*, 12663–12672.

Li, C., Iscen, A., Sai, H., Sato, K., Sather, N., Chin, A.S.M., Álvaroez, Z., Palmer, L.C., Schatz, G.C., and Stupp, S.I. (2020). Supramolecular–covalent hybrid polymers for light-activated mechanical actuation. Nat. Mater. *19*, 900–909.

Liu, J.-J., Hong, Y.-J., Guan, Y.-F., Lin, M.-J., Huang, C.-C., and Dai, W.-X. (2015). Lone pair–π interaction-induced generation of non-interpenetrated and photochromic cuboid 3-D naphthalene diimide coordination networks. Dalton Trans. *44*, 653–658.

Liu, L., Liu, Q., Li, R., Wang, M.-S., and Guo, G.-C. (2021). Controlled photoinduced generation of "visual" partially and fully charge separated states in viologen analogues. J. Am. Chem. Soc. *143*, 2232–2238.

Long, S., Bi, S., Liao, Y., Xue, Z., and Xie, X. (2014). Concurrent solution-like decoloration rate and high mechanical strength from polymer-dispersed photochromic organogel. Macromol. Rapid Commun. *35*, 741–746.

Ma, Z., Li, A., Huang, L., Qiu, Y., Xu, S., Xu, W., and Jia, X. (2019). Photochromism of aminobenzopyrano-xanthene with different fluorescent behavior in solution and the crystal state. J. Mater. Chem. C *7*, 275–280.

Ma, Y., Yu, Y., She, P., Lu, J., Liu, S., Huang, W., and Zhao, Q. (2020a). On-demand regulation of photochromic behavior through various counterions for high-level security printing. Sci. Adv. *6*, eaaz2386.

Ma, Y.-J., Hu, J.-X., Han, S.-D., Pan, J., Li, J.-H., and Wang, G.-M. (2020b). Manipulating on/off single-molecule magnet behavior in a Dy(III)-based photochromic complex. J. Am. Chem. Soc. *142*, 2682–2689.

McCracken, J.M., Donovan, B.R., and White, T.J. (2020). Materials as machines. Adv. Mater. *32*, 1906564.

McCune, J.A., Mommer, S., Parkins, C.C., and Scherman, O.A. (2020). Design principles for aqueous interactive materials: lessons from small molecules and stimuli-responsive systems. Adv. Mater. *32*, 1906890.

Meldrum, F.C., and O'Shaughnessy, C. (2020). Crystallization in confinement. Adv. Mater. *32*, 2001068. 1.

Merindol, R., and Walther, A. (2017). Materials learning from life: concepts for active, adaptive and autonomous molecular systems. Chem. Soc. Rev. *46*, 5588–5619.

Morin, S.A., Shepherd, R.F., Kwok, S.W., Stokes, A.A., Nemiroski, A., and Whitesides, G.M. (2012). Camouflage and display for soft machines. Science *337*, 828–832.

Moulin, E., Faour, L., Carmona-Vargas, C.C., and Giuseppone, N. (2020). From molecular machines to stimuli-responsive materials. Adv. Mater. *32*, 1906036.

Orgiu, E., and Samorì, P. (2014). 25th anniversary article: organic electronics marries photochromism: generation of multifunctional interfaces, materials, and devices. Adv. Mater. *26*, 1827–1845.

Priimagi, A., and Hecht, S. (2020). From responsive molecules to interactive materials. Adv. Mater. *32*, 2000215.

Samanta, D., Galaktionova, D., Gemen, J., Shimon, L.J.W., Diskin-Posner, Y., Avram, L., Král, P., and Klajn, R. (2018). Reversible chromism of spiropyran in the cavity of flexible coordination cage. Nat. Commun. *9*, 641.

Song, Q., Li, F., Wang, Z., and Zhang, X. (2015). A supramolecular strategy for tuning the energy level of naphthalenediimide: promoted formation of radical anions with extraordinary stability. Chem. Sci. *6*, 3342–3346.

Štacko, P., Kistemaker, J.C.M., Leeuwen, T., Chang, M.-C., Otten, E., and Feringa, B.L. (2017). Locked synchronous rotor motion in a molecular motor. Science *356*, 964–968.

Sun, L., Wang, Y., Yang, F., Zhang, X., and Hu, W. (2019). Cocrystal engineering: a collaborative strategy toward functional materials. Adv. Mater. *31*, 1902328.

Teyssier, J., Saenko, S.V., Marel, D., and Milinkovitch, M.C. (2015). Photonic crystals cause active colour change in chameleons. Nat. Commun. *6*, 6368.

Torres-Pierna, H., Ruiz-Molinab, D., and Roscini, C. (2020). Highly transparent photochromic films with a tunable and fast solution-like response. Mater. Horiz. *7*, 2749–2759.

Usui, R., Yamamoto, K., Okajima, H., Mutoh, K., Sakamoto, A., Abe, J., and Kobayashi, Y. (2020). Photochromic radical complexes that show heterolytic bond dissociation. J. Am. Chem. Soc. *142*, 10132–10142.

Vázquez-Mera, N., Roscini, C., Hernando, J., and Ruiz-Molina, D. (2013). Liquid-filled capsules as fast responsive photochromic materials. Adv. Opt. Mater. *1*, 631–636.

Walther, A. (2020). Viewpoint: from responsive to adaptive and interactive materials and materials systems: a roadmap. Adv. Mater. *32*, 1905111.

Wang, L., and Li, Q. (2018). Photochromism into nanosystems: towards lighting up the future nanoworld. Chem. Soc. Rev. *47*, 1044–1097.

White, T.J., and Broer, D.J. (2015). Programmable and adaptive mechanics with liquid crystal polymer networks and elastomers. Nat. Mater. *14*, 1087–1098.

Williams, D.E., Martin, C.R., Dolgopolova, E.A., Swifton, A., Godfrey, D.C., Ejegbavwo, O.A., Pellechia, P.J., Smith, M.D., and Shustova, N.B. (2018). Flipping the switch: fast photoisomerization in a confined environment. J. Am. Chem. Soc. *140*, 7611–7622.

Xu, C., Stiubianu, G.T., and Gorodetsky, A.A. (2018). Adaptive infrared-reflecting systems inspired by cephalopods. Science *359*, 1495–1500.

Yoreo, J.J.D., Gilbert, P.U.P.A., Sommerdijk, N.A.J.M., Penn, R.L., Whitelam, S., Joester, D., Zhang, H., Rimer, J.D., Navrotsky, A., Banfield, J.F., et al. (2015). Crystallization by particle attachment in synthetic, biogenic, and geologic environments. Science *349*, 498.

Zhang, J., Zhou, Q., and Tian, H. (2013). Photochromic materials: more than meets the eye. Adv. Mater. *25*, 378–399.

Zhang, J., Fu, Y., Han, H.-H., Zang, Y., Li, J., He, X.-P., Feringa, B.L., and Tian, H. (2017). Remote light-controlled intracellular target recognition by photochromic fluorescent glycoprobes. Nat. Commun. *8*, 987.

Zhang, X., Chen, L., Lim, K.H., Gonuguntla, S., Lim, K.W., Pranantyo, D., Yong, W.P., Yam, W.J.T., Low, Z., Teo, W.J., et al. (2019). The pathway to intelligence: using stimuli-responsive materials as building blocks for constructing smart and functional systems. Adv. Mater. *31*, 1804540.

STAR★METHODS

KEY RESOURCES TABLE

REAGENT or RESOURCE	SOURCE	IDENTIFIER
Chemical regents		
N,N-Dimethylformamide (DMF)	Aladdin regent corporation	CAS: 68-12-2
N,N-Dimethylacetamide (DMA)	Aladdin regent corporation	CAS: 127-19-5
1,4,5,8-naphthalene-tetracarboxylic dianhydride	Energy Chemical	CAS: 81-30-1
4-amino pyridine	J&K scientific Ltd	CAS: 504-24-5
Poly(methyl methacrylate) (PMMA)	Aladdin regent corporation	CAS: 9011-14-7
Deposited data		
DMA-NDI	This paper; Cambridge Crystallographic Data Center	CCDC: 1978948
Software and algorithms		
Gaussian 09	Frisch et al. (2009)	http://gaussian.com
Diamond 3.0	Crystal Impact	http://www.crystalimpact.com/diamond/Default.htm
ChemDraw Professional 14.0	PerkinElmer	https://www.perkinelmer.com/category/chemdraw
Mercury 2021.1	The Cambridge Crystallographic Data Centre	https://www.ccdc.cam.ac.uk/solutions/csd-core/components/mercury/

RESOURCE AVAILABILITY

Lead contact

Further information and requests for resources should be directed to and will be fulfilled by the lead contact, Can-Zhong Lu (czlu@fjirsm.ac.cn).

Materials availability

All materials generated in this study are available from the lead contact without restriction.

Data and code availability

Crystal data for **DMA-NDI** are available from the Cambridge Crystallographic Data Centre under CCDC: 1978948. Computational output is available on request. Any additional information required to reanalyze the data reported in this paper is available from the lead contact upon request.

METHOD DETAILS

Synthesis and preparation

Preparation of DMA-NDI cocrystal. The ligand NDI was prepared according to the reference (Dinolfo et al., 2004). The NDI (225 mg) was dissolved in DMA (40 ml) in a 50-ml beaker and covered with polyethylene preservative film with ultrasonic dissolution. The resulting saturated solution was sealed and stored in dark for two weeks under ambient condition. Then colorless needle-like crystals formed on the bottom of the beaker. The formula of the crystal was determined to be $(NDI)_2 \cdot (DMA)_2$ on the basis of the combined results of X-ray single-crystal structure analysis and elemental analysis. Elemental analysis: Calculated (%), C: 66.27, H: 4.17, N: 13.8; Found (%), C: 64.41, H: 3.4, N: 12.48. Infrared (single crystal, cm^{-1}) 3375(w), 3066(w), 3036(w), 2930(w), 1997(w), 1713 (s), 1668(s), 1635(s), 1577(s), 1494(w), 1449(s), 1412(m), 1341(s), 1242(s), 1197(s), 1148(m), 1119(m), 1065(m), 987(s), 884(m), 863(m), 826(m), 765(s), 750(s), 719(s), 580(m).

Preparation of the doped transparent polymeric film. In a 20-ml glass vial, commercially available PMMA (1g, 98.5wt%) was dissolved in 5 ml of DMA, and then DMA-NDI organic solid (15 mg, 1.5 wt%)

was added to the transparent polymeric solution with ultrasonic irradiation and further heated at 100°C for an hour to obtain homogeneous photochromic polymeric solution. A dropper was used to suck the polymeric solution and evenly applied onto the clean glass slide. The solvent was allowed to dry under vacuum for 8 hours at 60°C, after which a solid and transparent polymeric film was obtained.

Characterizations

Thermogravimetric analysis (TGA) experiment was performed on a Mettler Toledo TGA/DSC 1 STAR system instrument at a heating rate of 5°C/min under nitrogen atmosphere. PXDR measurements were recorded on a Rigaku Miniflex 600 X-ray diffractometer using Cu-K_α radiation. Elemental analyses for C, H, and N were obtained on Elementer Vario EL cube. FT-IR spectra were measured using a Thermo Nicolet is 50 FT-IR spectrophotometer. UV-vis absorption and diffuse reflectance spectra were recorded on a PerkinElmer Lambda-950 UV/Vis/NIR spectrophotometer. For diffuse reflectance, spectra were recorded with an integrating sphere. ESR spectra were recorded on a Bruker BioSpin E500 ESR spectrometer with a 100-KHz magnetic field. Ahigh-power xenon light source was used for stimulated sunlight with MICROSOLAR300.

X-ray crystallography

The as-synthesized crystals of **DMA-NDI** was coated with oil and placed on top of a nylon cryoloop and then mounted in the diffractometer. Single-crystal X-ray diffraction data were collected on a BRUKER APEX-II CCD rotating anode diffractometer equipped with focusing mirrors with Mo K_α (λ = 0.71073 Å) radiation under cryogenic conditions, which are controlled with a cryostat system equipped with a N_2 generator. The structure was solved by direct methods and was refined by the least-squares method with SHELXL-2018 program package. All non-hydrogen atoms were refined with anisotropic displacement parameters. Hydrogen atoms of the ligands were located by geometrical calculations, and their positions and thermal parameters were fixed during structural refinement.

Crystal data for **DMA-NDI**: $C_{56}H_{42}N_{10}O_{10}$ (M =1014.99 g/mol): triclinic, space group P-1 (no. 2), a = 5.1465(2) Å, b = 21.3321(10) Å, c = 22.0169(11) Å, α = 96.675(2)°, β = 90.570(2)°, γ = 91.999(2)°, V = 2399.06(19) $Å^3$, Z = 2, T = 150(2) K, μ(MoK_α) = 0.099 mm^{-1}, D_{calc} = 1.405 g/cm^3, 93662 reflections measured (3.988° $\leq 2\theta \leq$ 55.026°), 11049 unique (R_{int} = 0.0766, R_{sigma} = 0.0416) which were used in all calculations. The final R_1 was 0.0536 ($I > 2\sigma(I)$) and wR_2 was 0.1512 (all data) (Table S1). CCDC 1978948 (DMA-NDI) contains the supplementary crystallographic data for this study. The data can be obtained free of charge from the Cambridge Crystallographic Data Centre via www.ccdc.cam.ac.uk/data_request/cif.

UV/visible and NIR spectroscopy

(i) ***In situ* dynamic UV-visible absorption spectra upon photo irradiation in dilute solution state.**

UV-vis absorption spectra were recorded on a PerkinElmer Lambda-950 UV/Vis/NIR spectrophotometer. The UV/vis spectroscopic experiments were performed in a quartz cuvette with an optical path length of 1 cm. Dynamic UV/vis absorption spectra of NDI in DMA dilute solution with a concentration of 2×10^{-4}M were monitored upon photo irradiation using a 300-W xenon lamp for 3 minutes at 30-seconds intervals. With the prolongation of photo irradiation, the main peak at 360 nm and 379 nm progressively disappeared and a broad charge transfer absorption emerged from 395 nm to 550 nm.

(ii) ***In situ* solid-state UV-visible and near-IR diffuse reflectance spectra upon photo irradiation.**

Solid-state UV-vis near-IR diffuse reflectance spectra were recorded on a PerkinElmer Lambda-950 UV/vis/NIR spectrophotometer with an integrating sphere. The *in situ* dynamic solid-state diffuse reflectance spectra of **DMA-NDI** were recorder upon irradiation using a 300-W xenon lamp for 6 minutes at 1-minute intervals.

(iii) ***In situ* dynamic UV-visible and near-IR absorption spectra of the doped polymeric matrix upon photo irradiation.**

The UV-visible and near-IR absorption spectra of the NDI-doped polymeric films were recorded on a PerkinElmer Lambda-950 UV/Vis/NIR spectrophotometer. The *in situ* dynamic absorption spectra of NDI-doped polymeric film were recorded upon irradiation using a 300-W xenon lamp for 4 minutes.

Electron spin resonance spectroscopy

(i) **Dynamic ESR spectra in the solution state.**

ESR spectra were recorded on a Bruker BioSpin E500 ESR spectrometer with a 100-KHz magnetic field. The dynamic ESR spectra of the saturated solution (55 mg of NDI in 10 ml of DMA) were recorded upon irradiation using a 300-W xenon lamp for 50 seconds at 10-second intervals.

(ii) **Dynamic ESR spectra in the solid state with photo irradiation.**

The solid-state crystalline sample of **DMA-NDI** for dynamic photo irradiation ESR measurement was prepared by putting the sample in the ESR glass tube. The glass tube was sealed in a glove box under N_2 atmosphere and then placed on the EPR resonator. The *in situ* dynamic ESR spectra of the sample were recorded by irradiating using a 300-W xenon lamp for 14 minutes at 2-minute intervals.

(iii) **Dynamic ESR spectra in the solid state with variable temperature.**

The solid-state single-crystal sample of **DMA-NDI** for variable-temperature EPR measurement was performed by putting the single crystals in the EPR glass tube. The glass tube was sealed in a glove box under N_2 atmosphere and then placed on the EPR resonator. The *in situ* dynamic ESR spectra of the sample were recorded by controlling the temperature from 100 K to 400 K.

Dynamic fading curves of the NDI-doped polymeric film

To investigate the photochromic properties of the doped polymeric film, time-resolved UV-visible measurements were carried out using PerkinElmer Lambda-950 UV/Vis/NIR spectrophotometer at room temperature (25°C). Upon light irradiation for 1 minute by sunlight simulator (300W xenon lamp), the evolution of the transmittance of the colored brown polymeric film was immediately monitored by UV-visible time-resolved absorption spectroscopy at absorption band λ=472 nm. Figure S5 shows the fading curves of the photochromic polymeric film after ceasing irradiation in three hours. The decay curves for the transient absorbance were fitted by standard biexponential model: $A(t) = A_1e^{-k_1t} + A_2e^{-k_2t} + A_{th}$, where A(t) is the optical density at λ=472 nm and A_{th} is the optical density when time approaches infinity. k_1 and k_2 are the rate constants. According to the fitting function, $k_1=1.68\times10^{-3}s^{-1}$, and $k_2=1.51\times10^{-4}s^{-1}$. The half-live ($\tau_{1/2}$) of the doped polymeric film was estimated from the fitting curve of the time variation of the transient absorbance after the sunlight irradiation by biexponential function.

Computational details

For the studied complex, DFT is used to calculate the single-point energy and analyze the electronic structures. The functional B3LYP combining with the basis set 6-311+G(d,p) for C, H, N, and O atoms is adopted. The structure of the D-A molecular complex was directly imported from the crystal document. All the DFT calculations are carried out in the Gaussian 09 program package (Frisch et al., 2009). The DFT calculations demonstrate that the HOMO and LUMO of the complex are mainly distributed on the electron-donating molecule DMA and electron-accepting molecule NDI, respectively.

We use the polarizable continuum model (PCM) with the solvent parameters corresponding to DMA to describe the polarization effect in the crystal lattice. The calculated energy levels of HOMO and LUMO are -6.87eV and -3.74 eV, respectively. Therefore, the energy difference between HOMO and LUMO levels is about 3.13 eV in our simulations.